Frequency Drift in MR Spectroscopy at 3T.

S. C. N. Hui, M. Mikkelsen, H. J. Zöllner, V. Ahluwalia, S. Alcauter, L. Baltusis, D. A. Barany, L. R. Barlow, R. Becker, J. I. Berman, et al.

NeuroImage 241 (2021) 118430

Contents lists available at ScienceDirect

NeuroImage

journal homepage: www.elsevier.com/locate/neuroimage

Frequency drift in MR spectroscopy at 3T

Steve C.N. Hui[a,b], Mark Mikkelsen[a,b], Helge J. Zöllner[a,b], Vishwadeep Ahluwalia[c], Sarael Alcauter[d], Laima Baltusis[e], Deborah A. Barany[f], Laura R. Barlow[g], Robert Becker[h], Jeffrey I. Berman[i], Adam Berrington[j], Pallab K. Bhattacharyya[k], Jakob Udby Blicher[l], Wolfgang Bogner[m], Mark S. Brown[n], Vince D. Calhoun[o], Ryan Castillo[p], Kim M. Cecil[q], Yeo Bi Choi[r], Winnie C.W. Chu[s], William T. Clarke[t], Alexander R. Craven[u], Koen Cuypers[v,aq], Michael Dacko[w], Camilo de la Fuente-Sandoval[x], Patricia Desmond[y], Aleksandra Domagalik[z], Julien Dumont[aa], Niall W. Duncan[ab], Ulrike Dydak[ac], Katherine Dyke[ad], David A. Edmondson[q], Gabriele Ende[h], Lars Ersland[ae], C. John Evans[af], Alan S.R. Fermin[ag], Antonio Ferretti[ah], Ariane Fillmer[ai], Tao Gong[aj], Ian Greenhouse[ak], James T. Grist[al], Meng Gu[am], Ashley D. Harris[an], Katarzyna Hat[z1], Stefanie Heba[ao], Eva Heckova[m], John P. Hegarty II[ap], Kirstin-Friederike Heise[aq], Shiori Honda[cp], Aaron Jacobson[ar], Jacobus F.A. Jansen[as], Christopher W. Jenkins[af], Stephen J. Johnston[at], Christoph Juchem[au], Alayar Kangarlu[av], Adam B. Kerr[e], Karl Landheer[au], Thomas Lange[w], Phil Lee[aw], Swati Rane Levendovszky[ax], Catherine Limperopoulos[ay], Feng Liu[av], William Lloyd[az], David J. Lythgoe[ba], Maro G. Machizawa[ag], Erin L. MacMillan[g,cm], Richard J. Maddock[bb], Andrei V. Manzhurtsev[bc,bu], María L. Martinez-Gudino[bd], Jack J. Miller[be,co], Heline Mirzakhanian[ar], Marta Moreno-Ortega[av], Paul G. Mullins[bf], Shinichiro Nakajima[cp], Jamie Near[bg], Ralph Noeske[cn], Wibeke Nordhøy[bh], Georg Oeltzschner[a,b], Raul Osorio-Duran[bd], Maria C.G. Otaduy[bi], Erick H. Pasaye[d], Ronald Peeters[bj], Scott J. Peltier[bk], Ulrich Pilatus[bl], Nenad Polomac[bl], Eric C. Porges[bm], Subechhya Pradhan[ay], James Joseph Prisciandaro[bn], Nicolaas A Puts[bo], Caroline D. Rae[p], Francisco Reyes-Madrigal[x], Timothy P.L. Roberts[i], Caroline E. Robertson[r], Jens T. Rosenberg[bp], Diana-Georgiana Rotaru[ba], Ruth L O'Gorman Tuura[bq], Muhammad G. Saleh[br], Kristian Sandberg[l], Ryan Sangill[l], Keith Schembri[bs], Anouk Schrantee[bt], Natalia A. Semenova[bc,bu], Debra Singel[bv], Rouslan Sitnikov[bw], Jolinda Smith[bx], Yulu Song[aj], Craig Stark[by], Diederick Stoffers[bz], Stephan P. Swinnen[aq], Rongwen Tain[by], Costin Tanase[bb], Sofie Tapper[a,b], Martin Tegenthoff[ao], Thomas Thiel[ca], Marc Thioux[cb], Peter Truong[cc], Pim van Dijk[cb], Nolan Vella[bs], Rishma Vidyasagar[cd], Andrej Vovk[ce], Guangbin Wang[aj], Lars T. Westlye[bh], Timothy K. Wilbur[ax], William R. Willoughby[cf], Martin Wilson[cg], Hans-Jörg Wittsack[ch], Adam J. Woods[bm], Yen-Chien Wu[ci], Junqian Xu[cj], Maria Yanez Lopez[ck], David K.W. Yeung[s], Qun Zhao[cl], Xiaopeng Zhou[ac], Gasper Zupan[ce], Richard A.E. Edden[a,b,*]

[a] *Russell H. Morgan Department of Radiology and Radiological Science, The Johns Hopkins University School of Medicine, Baltimore, MD, USA*
[b] *F. M. Kirby Research Center for Functional Brain Imaging, Kennedy Krieger Institute, Baltimore, MD, USA*
[c] *GSU/GT Center for Advanced Brain Imaging, Georgia Institute of Technology, Atlanta, GA USA*
[d] *Instituto de Neurobiología, Universidad Nacional Autónoma de México, Queretaro, Mexico*
[e] *Center for Cognitive and Neurobiological Imaging, Stanford University, Stanford, CA USA*
[f] *Department of Kinesiology, University of Georgia, and Augusta University/University of Georgia Medical Partnership, Athens, GA USA*

* Corresponding author. Division of Neuroradiology, Park 367H, The Johns Hopkins University School of Medicine, 600 N Wolfe St, Baltimore, MD 21287, USA.
E-mail address: raee2@jhu.edu (R.A.E. Edden).

https://doi.org/10.1016/j.neuroimage.2021.118430.
Received 26 March 2021; Received in revised form 18 June 2021; Accepted 22 July 2021
Available online 24 July 2021.

[g] Department of Radiology, Faculty of Medicine, The University of British Columbia, Vancouver, Canada
[h] Center for Innovative Psychiatry and Psychotherapy Research, Department Neuroimaging, Central Institute of Mental Health, Medical Faculty Mannheim, Heidelberg University, Mannheim, Germany
[i] Department of Radiology, Children's Hospital of Philadelphia, Philadelphia, PA USA
[j] Sir Peter Mansfield Imaging Centre, School of Physics and Astronomy, University of Nottingham, Nottingham, UK
[k] Imaging Institute, The Cleveland Clinic, Cleveland, OH USA
[l] Center of Functionally Integrative Neuroscience, Aarhus University, Aarhus, Denmark
[m] Department of Biomedical Imaging and Image-guided Therapy, High-Field MR Center, Medical University of Vienna, Vienna, Austria
[n] Department of Radiology, Medical Physics, University of Colorado Anschutz Medical Campus, Aurora, CO, USA
[o] Tri-Institutional Center for Translational Research in Neuroimaging and Data Science (TReNDS), Georgia State University, Georgia Institute of Technology, and Emory University, Atlanta, GA USA
[p] NeuRA Imaging, Neuroscience Research Australia, Randwick, Australia
[q] Department of Radiology, Cincinnati Children's Hospital Medical Center, Cincinnati, OH USA
[r] Department of Psychological and Brain Sciences, Dartmouth College, Hanover, NH USA
[s] Department of Imaging and Interventional Radiology, The Chinese University of Hong Kong, Hong Kong, China
[t] Wellcome Centre for Integrative Neuroimaging, FMRIB, Nuffield Department of Clinical Neurosciences, University of Oxford, Oxford, UK
[u] Department of Biological and Medical Psychology, University of Bergen, Haukeland University Hospital, Bergen, Norway
[v] REVAL Rehabilitation Research Institute (REVAL), Hasselt University, Diepenbeek, Belgium
[w] Department of Radiology, Medical Physics, Medical Center - University of Freiburg, Faculty of Medicine, University of Freiburg, Freiburg, Germany
[x] Laboratory of Experimental Psychiatry & Neuropsychiatry Department, Instituto Nacional de Neurología y Neurocirugía, Mexico City, Mexico
[y] Department of Radiology, University of Melbourne/ Royal Melbourne Hospital, Melbourne, Australia
[z] Brain Imaging Core Facility, Malopolska Centre of Biotechnology, Jagiellonian University, Kraków, Poland
[z1] Consciousness Lab, Institute of Psychology, Jagiellonian University, Kraków, Poland
[aa] Univ. Lille, CNRS, Inserm, CHU Lille, Institut Pasteur de Lille, US 41 - UMS 2014 - PLBS, F-59000 Lille, France
[ab] Graduate Institute of Mind, Brain and Consciousness, Taipei Medical University, Taipei, Taiwan
[ac] School of Health Sciences, Purdue University, West Lafayette, IN USA
[ad] School of Psychology, University of Nottingham, Nottingham, UK
[ae] Department of Clinical Engineering, University of Bergen, Haukeland University Hospital, Bergen, Norway
[af] CUBRIC, Cardiff university, Cardiff, Wales, UK
[ag] Center for Brain, Mind and KANSEI Sciences Research, Hiroshima University, Hiroshima, Japan
[ah] Department of Neuroscience, Imaging and Clinical Sciences, University "G. d'Annunzio" of Chieti-Pescara, Chieti, Italy
[ai] Physikalisch-Technische Bundesanstalt (PTB), Braunschweig und Berlin, Germany
[aj] Department of Imaging and Nuclear Medicine, Shandong Medical Imaging Research Institute, Shandong University, Jinan, China
[ak] Department of Human Physiology, University of Oregon, Eugene, OR USA
[al] Department of Physiology, Anatomy, and Genetics, Oxford Centre for Magnetic Resonance / Department of Radiology, The Churchill Hospital, The University of Oxford, Oxford, UK
[am] Department of Radiology, Stanford University, Stanford, CA, USA
[an] Department of Radiology, University of Calgary, Calgary, Canada
[ao] Department of Neurology, BG University Hospital Bergmannsheil, Bochum, Germany
[ap] Department of Psychiatry & Behavioral Sciences, Stanford University, Stanford, CA, USA
[aq] Department of Movement Sciences, KU Leuven, Leuven, Belgium
[ar] Department of Radiology / Psychiatry, University of California San Diego, San Diego, CA USA
[as] Department of Radiology and Nuclear Medicine, Maastricht University Medical Center, Maastricht, The Netherlands
[at] Psychology Department / Clinical Imaging Facility, Swansea University, Swansea, UK
[au] Departments of Biomedical Engineering and Radiology, Columbia University, New York, NY USA
[av] Department of Psychiatry, Columbia University Irving Medical Center/New York State Psychiatric Institute, New York, NY USA
[aw] Department of Radiology / Hoglund Biomedical Imaging Center, University of Kansas Medical Center, Kansas City, KS USA
[ax] Department of Radiology, University of Washington, Seattle, WA USA
[ay] Developing Brain Institute, Diagnostic Imaging and Radiology, Children's National Hospital, Washington, DC USA
[az] Division of Informatics, Imaging & Data Sciences, University of Manchester, Manchester, UK
[ba] Department of Neuroimaging, Institute of Psychiatry, Psychology & Neuroscience, King's College London, London, UK
[bb] Department of Psychiatry and Behavioral Sciences, University of California Davis, Imaging Research Center, Davis, CA USA
[bc] Department of Radiology, Clinical and Research Institute of Emergency Pediatric Surgery and Trauma, Moscow, Russia
[bd] Departamento de Imágenes Cerebrales, Instituto Nacional de Psiquiatría Ramón de la Fuente Muñiz, Mexico City, Mexico
[be] Department of Physics, University of Oxford, Oxford, UK
[co] The MR Research Centre & The PET Research Centre, Aarhus University, Aarhus, DK
[bf] Bangor Imaging Unit, Department of Psychology, Bangor University, Bangor, Wales, UK
[bg] Douglas Mental Health University Institute and Department of Psychiatry, McGill University, Montreal, Canada
[bh] NORMENT, Division of Mental Health and Addiction and Department of Diagnostic Physics, Division of Radiology and Nuclear Medicine, Oslo University Hospital / Department of Psychology, University of Oslo, Oslo, Norway
[bi] LIM44, Instituto e Departamento de Radiologia, Faculdade de Medicina, Universidade de Sao Paulo, Sao Paulo, SP, Brazil
[bj] Department of Imaging & Pathology, Department of Radiology, University Hospitals Leuven, KU Leuven, Leuven, Belgium
[bk] Functional MRI Laboratory, University of Michigan, Ann Arbor, MI USA
[bl] Institute of Neuroradiology, Goethe-University Frankfurt, Frankfurt, Germany
[bm] Center for Cognitive Aging and Memory, McKnight Brain Institute, Department of Clinical and Health Psychology, College of Public Health and Health Professions. Department of Neuroscience, College of Medicine, University of Florida, Gainesville, USA
[bn] Department of Psychiatry and Behavioral Sciences, Medical University of South Carolina, Charleston, SC USA
[bo] Department of Forensic & Neurodevelopmental Sciences, Sackler Institute for Translational Neurodevelopment, King's College London, London, UK
[bp] McKnight Brain Institute, AMRIS, University of Florida, Gainesville, FL USA
[bq] Center for MR Research, University Children's Hospital, Zurich, University of Zurich, Switzerland
[br] Department of Diagnostic Radiology and Nuclear Medicine, University of Maryland School of Medicine, Baltimore, USA
[bs] Medical Physics, Mater Dei Hospital, Imsida, Malta
[bt] Department of Radiology and Nuclear Medicine, Amsterdam University Medical Center, University of Amsterdam, Amsterdam, The Netherlands
[bu] Emanuel Institute of Biochemical Physics of the Russian Academy of Sciences, Moscow, Russia
[bv] Department of Psychiatry, University of Colorado Anschutz Medical Campus, Aurora, CO, USA
[bw] Clinical Neuroscience, MRI Centre, Karolinska Institute, Stockholm, Sweden
[bx] Lewis Center for Neuroimaging, University of Oregon, Eugene, OR USA
[by] Department of Neurobiology and Behavior, Facility for Imaging and Brain Research (FIBRE) & Campus Center for Neuroimaging (CCNI), School of Biological Sciences, University of California, Irvine, Irvine, CA USA
[bz] Spinoza Centre for Neuroimaging, Royal Netherlands Academy of Arts and Sciences, Amsterdam, The Netherlands

[ca] Institute of Clinical Neuroscience and Medical Psychology, University Dusseldorf, Medical Faculty, Düsseldorf, Germany
[cb] Department of Otorhinolaryngology, Head and Neck Surgery, University of Groningen, University Medical Center Groningen, Groningen, The Netherlands
[cc] Brain Health Imaging Centre, Centre for Addiction and Mental Health, Toronto, Canada
[cd] Melbourne Dementia Research Centre, Florey Institute of Neurosciences and Mental Health, Melbourne, Australia
[ce] Faculty of Medicine, University of Ljubljana, Ljubljana, Slovenia
[cf] Department of Radiology, University of Alabama at Birmingham, Birmingham, AL USA
[cg] Centre for Human Brain Health and School of Psychology, University of Birmingham, Birmingham, UK
[ch] Department of Diagnostic and Interventional Radiology, University Düsseldorf, Medical Faculty, Düsseldorf, Germany
[ci] Department of Radiology, TMU-Shuang Ho Hospital, New Taipei City, Taiwan
[cj] Department of Radiology and Psychiatry, Baylor College of Medicine, Houston, USA
[ck] Perinatal Imaging & Health, King's College London, London, UK
[cl] Bioimaging Research Center, Department of Physics and Astronomy, University of Georgia, Athens, GA USA
[cm] Philips Canada, Markham, ON, Canada
[cn] GE Healthcare, Berlin, Germany
[cp] Department of Neuropsychiatry, Keio University School of Medicine, Tokyo, Japan

ARTICLE INFO

Keywords:
Magnetic resonance spectroscopy (MRS)
Frequency drift
3T
Press
Multi-vendor
Multi-site

ABSTRACT

Purpose: Heating of gradient coils and passive shim components is a common cause of instability in the B_0 field, especially when gradient intensive sequences are used. The aim of the study was to set a benchmark for typical drift encountered during MR spectroscopy (MRS) to assess the need for real-time field-frequency locking on MRI scanners by comparing field drift data from a large number of sites.

Method: A standardized protocol was developed for 80 participating sites using 99 3T MR scanners from 3 major vendors. Phantom water signals were acquired before and after an EPI sequence. The protocol consisted of: minimal preparatory imaging; a short pre-fMRI PRESS; a ten-minute fMRI acquisition; and a long post-fMRI PRESS acquisition. Both pre- and post-fMRI PRESS were non-water suppressed. Real-time frequency stabilization/adjustment was switched off when appropriate. Sixty scanners repeated the protocol for a second dataset. In addition, a three-hour post-fMRI MRS acquisition was performed at one site to observe change of gradient temperature and drift rate. Spectral analysis was performed using MATLAB. Frequency drift in pre-fMRI PRESS data were compared with the first 5:20 minutes and the full 30:00 minutes of data after fMRI. Median (interquartile range) drifts were measured and showed in violin plot. Paired t-tests were performed to compare frequency drift pre- and post-fMRI. A simulated in vivo spectrum was generated using FID-A to visualize the effect of the observed frequency drifts. The simulated spectrum was convolved with the frequency trace for the most extreme cases. Impacts of frequency drifts on NAA and GABA were also simulated as a function of linear drift. Data from the repeated protocol were compared with the corresponding first dataset using Pearson's and intraclass correlation coefficients (ICC).

Results: Of the data collected from 99 scanners, 4 were excluded due to various reasons. Thus, data from 95 scanners were ultimately analyzed. For the first 5:20 min (64 transients), median (interquartile range) drift was 0.44 (1.29) Hz before fMRI and 0.83 (1.29) Hz after. This increased to 3.15 (4.02) Hz for the full 30 min (360 transients) run. Average drift rates were 0.29 Hz/min before fMRI and 0.43 Hz/min after. Paired t-tests indicated that drift increased after fMRI, as expected ($p < 0.05$). Simulated spectra convolved with the frequency drift showed that the intensity of the NAA singlet was reduced by up to 26%, 44 % and 18% for GE, Philips and Siemens scanners after fMRI, respectively. ICCs indicated good agreement between datasets acquired on separate days. The single site long acquisition showed drift rate was reduced to 0.03 Hz/min approximately three hours after fMRI.

Discussion: This study analyzed frequency drift data from 95 3T MRI scanners. Median levels of drift were relatively low (5-min average under 1 Hz), but the most extreme cases suffered from higher levels of drift. The extent of drift varied across scanners which both linear and nonlinear drifts were observed.

1. Introduction

MRI scanners rely upon a strong magnetic field (B_0) in order to polarize the bulk magnetization of ^1H protons and generate detectable radiofrequency (RF) signals. Magnetic field gradient pulses allow the encoding of position as the resonance frequency is linearly proportional to the magnetic field. Hence, gradient pulses are used to make RF pulses slice-selective, to suppress unwanted signals, and to directly read out the location of signals during acquisition. Rapid switching of gradient fields, which is a common feature of efficient modern imaging sequences, results in the deposition of substantial amounts of energy within the scanner. Eddy currents release heat between vibrating parts in the coil system, heating up the nearby heat shield and shimming elements (El-Sharkawy et al., 2006; Foerster et al., 2005). Although the gradient coils themselves are water-cooled, vibrations and eddy currents that they induce deposit energy elsewhere in the scanner that is less efficiently temperature-controlled, changing the local temperature of conducting scanner components. Unstable internal temperature leads to temperature-dependent changes in magnetic susceptibility and thus the B_0 field (Foerster et al., 2005).

Instability in the B_0 magnetic field can impact experiments in several ways. Firstly, experiments often rely upon frequency-selective pulses, including for positional and chemical-shift selectivity. Secondly, detected signals will be distorted by short-term B_0 instabilities during the acquisition window. Thirdly, longer-term B_0 instabilities will interfere with the appropriate combination of signals acquired during different TRs. Typically, slice-selective pulses are applied with high bandwidth and the location of signals is only minimally shifted by B_0 instability. In time-series fMRI, significant SNR loss due to gradient-induced heat drift can be recovered by realignment correction (Lange et al., 2011). However, MR spectroscopy (MRS) and imaging applications, which include chemical exchange saturation transfer imaging (CEST) and lipid suppression, make use of chemical-shift-selective pulses of narrower bandwidth, and hence will be more adversely impacted by B_0 instability (Poblador Rodriguez et al., 2019). Thus, B_0 instability particularly impacts MRS experiments, which rely upon extensive signal averaging, leading to in-

coherent averaging, line-broadened, distorted peaks and reduced SNR (Foerster et al., 2005; Henry et al., 1999; Rowland et al., 2017).

The magnitude of gradient-induced B_0 field changes varies depending on the length of the applied imaging protocol and the gradient duty cycle of the sequences, particularly when echo planar imaging (EPI) is used for e.g. fMRI and diffusion tensor imaging (DTI). In addition, scanner design characteristics including the amount and distribution of iron used in the passive shim elements plays a role in the B_0 field changes (Lange et al., 2011). It has been reported that up to ten hours were required for B_0 to return to its initial value after a two-hour fMRI acquisition (Foerster et al., 2005). B_0 field drift changes have a particular impact on *J*-difference approaches that rely on alignment and subtraction of individual transients, as is the case for e.g. MEGA–editing of GABA. One study reported frequency drift rates of over 1 Hz/min after 8 min of fMRI (Harris et al., 2014), compared to under 0.1 Hz/min without prior imaging and showed drift was associated with a 16% decrease in the GABA+ signal as measured with the respective edited MRS acquisition. This change in metabolite signal can be explained by the shifted position of frequency-selective editing pulses that characterize editing, targeting the scalar-coupled GABA resonances at 1.89 ppm and measurement of the observed signal at 3.01 ppm (Edden et al., 2012). A comparable field drift has also been observed after a 22- minute DTI acquisition, which resulted in an over 3 Hz/min drift after DTI compared to under 1 Hz/min without a previous DTI scan (Rowland et al., 2017). The narrow bandwidth of editing pulses makes frequency drift influential on both the efficiency of the editing experiment and the summation and subtraction of sub-spectra (Edden and Barker, 2007; van der Veen et al., 2017).

Given the particular impact of field drift on MRS, much work has sought to mitigate the impact of field drift on data through both prospective and retrospective approaches. The line-broadening and SNR losses caused by incoherent averaging of signals acquired with different B_0 frequencies can be addressed to a large extent by retrospective frequency correction during post-processing, which is now a consensus-recommended step in all MRS processing (Near et al., 2020; Wilson et al., 2019). Corrections via residual water signals, creatine referencing, spectral registration and non-water-suppressed methods have comparable efficacy on frequency correction (Ernst and Li, 2011; Helms and Piringer, 2001; Keating and Ernst, 2012; Near et al., 2015; van der Veen et al., 2017; Waddell et al., 2007; Wilson, 2019). In the residual water method, frequency shift and phase offset are corrected using the maximum water modulus and phase of the first point in the FID. In creatine referencing, the creatine peak is fitted to the real part of a Lorentzian using global nonlinear least squares with constrained parameters to achieve frequency and phase alignment. Spectral registration uses a representative average as a reference and fits other signal averages to this reference in the time domain using nonlinear least squares minimization. Non-water-suppressed acquisition techniques such as metabolite cycling offer the ability to improve frequency alignment in post-processing steps by aligning the high SNR water peak in each transient, but these acquisition methods have yet to be incorporated as product on clinical MRI systems. Nonetheless, many negative impacts of B_0 field drift cannot be removed by post-processing.

Prospective approaches such as a feedback-based interleaved reference scan (IRS) method utilize the water reference signal for a real-time update of the carrier frequency of RF pulses and analog-to-digital converter (Edden et al., 2016; Henry et al., 1999; Lange et al., 2011; Thiel et al., 2002). This feedback mechanism updates the water resonance on the basis of individual transients to prevent the water resonance from drifting in order to achieve drift correction. The IRS-based method has also been implemented in MRS imaging sequences for field drift and localization error correction (Ebel and Maudsley, 2005; Tal and Gonen, 2013). A more recent study proposed to obtain a localized reference using outer volume suppression localization and selective water excitation (Lee et al., 2018). This method prevents the saturation-induced SNR loss that happens in PRESS-based IRS navigators while also using the water peak as the reference for frequency drift correction. Difference-edited MRS, which relies upon accurate subtraction of large signals to resolve smaller ones, is particularly impacted by field drift, and the elimination of subtraction artifacts is an enduring challenge (Evans et al., 2013; Near et al., 2020; Waddell et al., 2007; Wilson et al., 2019). Water suppression pulses are often applied with narrow bandwidths in order to preserve signals around 4 ppm, and the size of the residual water signal can change dramatically after drift. The use of frequency-selective pulses is even more integral to edited MRS methods (Mullins et al., 2014), and if the resonant frequency of signals drifts away from the nominal frequency of editing pulses, losses in editing efficiency arise.

Frequency drift during either MRS or EPI-based acquisitions has rarely been studied especially on a large-scale multi-site and multi-vendor manner. Published works are mostly single-site and single-scanner studies which may not be representative to other scanners due to the use of different protocols and study design (Foerster et al., 2005; Harris et al., 2014; Rowland et al., 2017). The amount of frequency drift is scanner-dependent and related to the scanner's gradient coil system and cooling hardware that may vary across scanners. Such impact of drift may be reduced using prospective or retrospective frequency correction methods. However, efficacy of such corrections is poorly characterized and the impact of line-broadening, lineshape distortion, subtraction artifacts, and accuracy of frequency-selective pulses on spectral data collected from multiple scanners remains unclear. In this study, a standardized protocol was developed and shared across different sites with scanners from various vendors to study the impact of gradient-induced frequency drift and the consistency of drift within scanner. The aim of the standardized protocol was to reduce the number of confounding variables, allowing objective analysis of how EPI scanning influences frequency drift and how this may impact MR spectral analysis. By collecting data from a large number of sites worldwide, we aimed to establish a benchmark of the 'typical' levels of drift and to assess the need for real-time field-frequency locking (Henry et al., 1999). Each acquired dataset consisted of two sets of PRESS scans immediately before and after an EPI acquisition to characterize the B_0 field drift.

Table 1
Number of participating sites and data reported.

	Sites	Data reported (excluded)	Repeated data*
GE	21	22 (1)	15
Philips	23	30 (0)	20
Siemens	36	47 (3)	25
Total	80	99 (4)	60

* No repeated data were excluded.

2. Methods

2.1. Scanner details

Site recruitment was initiated from previous multi-site studies involving imaging centers focusing on neurological and psychological research with 3T scanners worldwide (Mikkelsen et al., 2017; Mikkelsen et al., 2019), and subsequently extended through advertising on social media. Eighty sites with 99 scanners were recruited (GE = 22, Philips = 30, Siemens = 47) and supplied data, of which 60 sites submitted two datasets acquired on separate days. Four sites with PET/MR scanners participated. See Table 1 for details.

2.2. Data acquisition

Sites were instructed to use a spherical or cylindrical water-dominant phantom, and a phased-array head or head-and-neck RF coil (between 8 and 64 channels). Scanning was performed following a period of at least 6h of scanner idle time (ideally the first scan of the day) to avoid any

Table 2
Scanner information for all datasets (n = 99).

Site ID	Scanner model	Software release	Year of install	Average hours of operation per day	Gradient max. amplitude (mT/m) / slew rate (T/m/s)	Mean absolute frequency offsets (Hz)		
						Pre-fMRI	Post-fMRI (5:20 min)	Post-fMRI (30:00 min)
G01a†	GE Discovery MR750	DV26	2010	12	50 / 200	0.30	0.16	1.66
G02a†	GE Discovery MR750	DV26	2019	1	50 / 200	0.14	0.19	1.66
G03a†	GE Discovery MR750	DV26	2014	9	50 / 200	0.05	0.16	1.47
G04a†	GE Discovery MR750	DV26	2010	11	50 / 200	0.08	0.68	2.46
G05a	GE Discovery MR750	DV26	2009	8	50m/ 200	0.14	1.11	3.44
G06a	GE Discovery MR750W	DV25	2013	6	44 / 200	0.46	3.46	5.88
G07a	GE Discovery MR750	DV26	2011	8	50 / 200	0.05	0.50	2.28
G08a	GE SIGNA Premier	RX27	2020	2	80 / 200	0.31	1.68	11.18
G09a†	GE SIGNA Premier	RX27	2018	8	80 / 200	0.13	0.76	4.11
G10a†	GE SIGNA UHP 3T	R27	2020	5	100 / 200	0.25	0.83	3.52
G11a†	GE SIGNA PET/MR	MP26	2016	5	44 / 200	0.36	2.20	4.20
G12a	GE Discovery MR750	DV25.1	2011	6	50 / 200	0.11	0.16	1.22
G15a†	GE Discovery MR750	DV26	2010	13	50 / 200	0.31	0.20	0.63
G16a†	GE Discovery MR750	DV26	2012	6	50 / 200	0.06	0.65	2.97
G17a†	GE Discovery MR750	DV25	2010	8	87 / 200	0.13	0.57	2.20
G18a†	GE SIGNA PET/MR	MP26	2014	4	44 / 200	0.30	1.00	1.20
G19a†	GE Discovery MR750	DV26	2011	8	50 / 200	0.28	0.52	2.45
G20a	GE Discovery MR750	DV26	2012	10	50 / 200	0.06	0.42	1.77
G21a#	GE SIGNA Premier	RX27	2019	10	80 / 200	n/a	n/a	n/a
G23a†	GE Discovery MR750	DV26	2016	5	50 / 200	0.04	0.50	2.56
G24a†	GE Discovery MR750	DV26	2012	6	50 / 200	0.14	0.54	2.34
G24b†	GE Discovery MR750	DV26	2013	6	50 / 200	0.06	1.04	3.75
P01a†	Philips Achieva	R5.6.1	2018	6	40 / 200	1.80	1.77	3.17
P01b†	Philips Ingenia	R5.6.1	2018	6	45 / 200	0.94	2.81	3.40
P02a†	Philips Achieva	R5.3.1.3	2012	14	80 / 100	1.42	3.63	5.63
P02b†	Philips Ingenia	R5.3.1.3	2015	8	45 / 200	0.65	1.75	2.70
P03a†	Philips Achieva	R5.6.1	2018	4	40 / 120	0.64	7.19	8.28
P03b†	Philips Ingenia	R5.6.1	2016	8	45 / 120	1.12	1.53	2.82
P04a	Philips Achieva TX	R5.6	2010	8	40 / 200	1.26	4.61	17.01
P05a†	Philips Achieva dStream	R5.7.1	2009	9	80 / 200	2.67	5.91	15.72
P06a	Philips Ingenia	R5.4.1.1	2016	8	45 / 200	1.14	1.42	1.56
P06b	Philips Achieva	R5.3.1.2	2010	8	80 / 100	1.97	1.47	6.88
P06c	Philips Ingenia Elition	R5.6.1	2018	8	45 / 220	1.02	1.69	1.96
P07a†	Philips Ingenia	R5.3.1.3	2017	6	80 / 200	0.13	0.45	4.96
P08a†	Philips ingenia Elition	R5.6.1	2020	3	45 / 220	0.93	4.23	3.62
P09a	Philips Ingenia	R5.4.1	2019	7	n/a	1.50	1.00	4.09
P10a	Philips Ingenia	R5.4.1	2016	8	80 / 200	0.07	0.44	5.65
P11a†	Philips Achieva	R5v30.02	2012	5	40 / 200	2.06	6.23	16.82
P12a†	Philips Ingenia	R5.6.1	2019	5	45 / 220	0.87	0.09	5.66
P13a†	Philips Achieva dStream	R5.6.1	2008	10	80 / 200	1.83	2.14	6.06
P15a†	Philips Ingenia Elition X	R5.6.1	2019	6	45 / 220	0.74	0.74	4.63
P16a	Philips Ingenia Elition X	R5.6.1	2020	2	45 / 220	1.05	0.23	8.07
P17a†	Philips Ingenia CX	R5.6.1	2019	2	40 / 200	1.40	0.63	1.67
P18a†	Philips Ingenia	R5.6.1	2012	9	33 / 200	0.83	2.43	7.69
P18b†	Philips Ingenia	R.5.61	2015	8	33 / 200	1.43	1.49	3.15
P18c†	Philips Ingenia Elition X	R.5.61	2018	9	45 / 200	1.35	2.50	2.10
P19a†	Philips Achieva	R5.4.1	2015	4	40 / 200	0.42	0.49	1.67
P20a†	Philips Achieva dStream	R5.4.0.1	2013	10	40 / 200	3.46	4.49	13.86
P22a	Philips Achieva dStream	R5.7.1	2020	8	45 / 200	0.44	0.72	5.82
P23a†	Philips Achieva	R5.4.1	2008	15	40 / 200	2.55	2.10	2.43
P24a	Philips Achieva	R5.6.1	2010	8	n/a	1.43	1.69	3.77
P25a	Philips Achieva	R3.3.2	2012	4	40 / 200	2.29	2.93	3.83
S01a†	Siemens Prisma	VE11B	2016	4	80 / 200	0.07	0.21	0.49
S02a#	Siemens Vida	XA20	2020	12	60 / 200	n/a	n/a	n/a
S03a†	Siemens Prisma	VE11C	2018	9	80 / 200	0.09	0.90	2.02
S03b†	Siemens Biograph mMR	VE11P	2017	5	45 / 200	0.53	0.81	2.26
S03c†	Siemens Trio	VB17	2006	4	45 / 200	0.04	0.60	0.87
S04a†	Siemens Skyra	VE11C	2015	8	45 / 200	1.80	0.34	7.71
S05a†	Siemens Prisma	VE11C	2018	4	80 / 200	0.03	0.05	0.56
S06a*	Siemens Prisma	VE11E	2019	8	40 / 200	0.03	0.22	0.93
S07a†	Siemens Biograph mMR	VE11P	2019	8	45 / 200	0.46	0.41	2.71
S07b†	Siemens Prisma	VE11E	2015	11	80 / 200	2.63	2.18	9.48
S08a†	Siemens Prisma	VE11C	2016	5	80 / 200	0.02	0.02	0.35
S09a†	Siemens Verio	VB17	2009	5	45 / 200	0.49	1.66	1.87
S10a	Siemens Prisma	VE11C	2020	3	80 / 200	0.02	0.02	0.34
S11a†*	Siemens Prisma	VE11C	2017	6	80 / 200	0.09	0.09	0.74
S11c†*	Siemens Prisma	VE11C	2015	3	80 / 200	0.09	0.11	0.22
S12a	Siemens Skyra	VE11E	2014	6	45 / 200	1.91	0.83	11.68
S13a*	Siemens Prisma	VE11C	2015	6	80 / 200	0.02	0.02	0.43
S13b*	Siemens Prisma	VE11C	2015	6	80 / 200	1.13	0.92	4.54
S13c*#	Siemens Connectom	VD13D	2015	6	300 / 200	n/a	n/a	n/a
S14a	Siemens Skyra	VD13A	2011	5	45 / 200	1.08	2.09	5.44

(*continued on next page*)

Table 2 (*continued*)

Site ID	Scanner model	Software release	Year of install	Average hours of operation per day	Gradient max. amplitude (mT/m) / slew rate (T/m/s)	Mean absolute frequency offsets (Hz)		
						Pre-fMRI	Post-fMRI (5:20 min)	Post-fMRI (30:00 min)
S15a†	Siemens Trio	VB19a	2007	5	45 / 200	0.02	0.90	1.71
S15b†	Siemens Prisma	VE11C	2002	10	80 / 200	0.11	1.49	3.90
S16a*	Siemens Skyra	VE11C	2012	9	45 / 200	0.47	1.65	3.23
S17a*	Siemens Skyra	VE11C	2019	3	45 / 200	0.19	0.38	4.74
S18a*	Siemens Tim Trio	VB17A	2009	8	45 / 200	0.03	0.14	0.21
S18b	Siemens Skyra	VE11C	2012	5	45 / 200	0.47	2.49	2.48
S19a*	Siemens Prisma	VE11C	2014	8	80 / 200	2.46	1.56	8.15
S20a†	Siemens Prisma	VE11C	2018	3	80 / 200	2.13	1.49	7.50
S21a†	Siemens Prisma	VE11C	2015	8	80 / 200	0.03	0.04	0.34
S22a*	Siemens Prisma	VE11C	2018	8	80 / 200	2.18	1.54	7.62
S22b*#	Siemens Skyra	VE11C	2020	12	45 / 200	n/a	n/a	n/a
S23a*	Siemens Prisma	VE11C	2016	8	80 / 200	1.66	1.24	5.70
S24a†	Siemens Prisma	VE11C	2016	8	80 / 200	2.30	2.25	11.39
S25a†	Siemens Prisma	VE11C	2016	8	80 / 200	0.04	0.10	0.13
S26a†*	Siemens Prisma	VE11C	2016	8	80 / 200	0.41	0.44	2.25
S27a†	Siemens Prisma	VE11C	2019	8	80 / 200	2.49	1.67	9.70
S27b†	Siemens Skyra	VE11C	2019	8	45 / 200	0.19	1.00	6.54
S28a*	Siemens Skyra	E11-A	2015	17	45 / 200	1.03	0.70	5.59
S29a†	Siemens Prisma	VE11E	2017	8	80 / 200	0.02	0.10	0.62
S30a†	Siemens Prisma	VE11C	2018	9	80 / 200	0.06	0.26	0.82
S31a	Siemens Prisma	VE11c	2015	9	80 / 200	2.36	1.67	8.13
S33a*	Siemens Prisma	VE11C	2016	9	80 / 200	0.05	0.06	0.51
S37a†	Siemens Prisma	VE11C	2016	3	80 / 200	0.08	0.64	0.33
S38a†	Siemens Prisma	VE11C	2016	9	80 / 200	0.23	0.76	2.54
S40a*	Siemens Prisma	VE11C	2017	8	80 / 200	0.08	0.13	0.94
S40b*	Siemens Prisma	VE11C	2015	8	80 / 200	3.29	2.36	10.21
S99a‡	Siemens Prisma	VE11C	2019	7	80 / 200	1.00	0.96	4.32

† indicates repeated protocol was performed.
* indicates chiller/eco mode was off. If not specify, the setting was in default.
# indicates data have been excluded due to noise artefact or headers unable to be read.
‡ indicates reassigned site ID for P21a.

drift confounds due to unintended heating effects from prior scanning. Phantoms were acclimatized in the scan room for the same period and positioned in the isocenter. Each site was required to submit a minimum of one dataset and suggested to repeat the protocol on a different day for a second dataset if possible. Phantom data files were shared securely and analyzed by the co-authors at the Johns Hopkins University School of Medicine with local IRB approval.

Raw data were exported in GE P-file (.7), Philips .data/.list and SDAT/SPAR and Siemens TWIX (.dat) formats as these formats contain the unaveraged information and, hence, allow for frequency and phase of individual transients to be observed. Data were uploaded to a secure online repository. Scanner details (i.e., date of scan, scanner vendor and model, software version, year of installation, estimated hours of use per day, coil, maximum gradient amplitude and gradient slew rate) were reported. Additional metrics including the course of the gradient temperature during the experiment and the number and bulk weight of passive shims were suggested to be included if available.

2.3. Scanning protocol

Unsuppressed water data were acquired from the phantom, using PRESS localization with real-time frequency stabilization/adjustment switched off, before and after a BOLD-weighted fMRI sequence. Standardized protocols were generated for GE, Philips and Siemens scanners consisting of: 1) minimal preparatory imaging; 2) pre-fMRI PRESS (TR/TE = 5000/35 ms; FA = 90°; 64 transients; no water suppression; voxel size = 2 × 2 × 2 cm^3; second-order shim; scan duration = 5:20 min); 3) BOLD-weighted EPI based on the ADNI-3 protocol (Weiner et al., 2017) (TR/TE = 3000/30 ms; 197 dynamics; EPI factor/echo train length = 31/64, Inter-echo times (echo spacing) 0.5 ms (GE and Philips) / 0.72 ms (Siemens) and FOV = 217×217 mm^2 (Philips and Siemens) / 220×220 mm^2 (GE), duration = 10 min); and 4) post-fMRI PRESS (same parameters as for pre-fMRI PRESS except 360 transients and duration = 30 min).

In addition, one GE site repeated the protocol with an extra-long acquisition, consisting of 16-min pre-fMRI PRESS (192 transients) and 171-minute post-fMRI PRESS (2048 transients) to investigate the time required for the frequency offset to reach a plateau. Except for the number of transients, all other parameters remained unchanged.

2.4. Data analysis

Data analyses were performed using MATLAB (R2020b, MathWorks, Natick, USA), including eddy-current correction (Klose, 1990) using the first acquired transient as a reference, zero-filling to yield an apparent spectral resolution of 0.24 Hz/point and Fourier transformation. The unsuppressed water peak in each transient of the pre- and post-fMRI PRESS spectra was modeled in the frequency domain using a Voigt lineshape function (Marshall et al., 1997) with a linear baseline to extract the water peak center frequency from each transient. Full-width half-maximum (FWHM) and the integral of the water signal were measured and reported to assess the change of lineshape. To compare frequency drift before and after fMRI, the mean absolute water peak frequency offset was calculated for each acquisition. Frequency offset was calculated as the difference between each transient's observed water signal frequency and the frequency of the first transient. The median drift is the median across the 95 datasets, of the mean offset throughout each measurement. Drift rate was measured pre-fMRI and over the same time period (5:20 min) of post-fMRI. The average drift rate is a mean across the 95 datasets which was calculated for each from the difference between the first and the last frequency offsets in Hz divided by the duration of the scan in minutes. Pearson's correlation coefficients (r) and two-sided paired t-tests were calculated between the mean absolute frequency offsets before and after fMRI for correlation and distribution

analyses. Spearman's rank correlation coefficients (ρ) were measured for the correlation of operating hours and years of usage with frequency offsets. Differences on operating hours and years of usage among vendors were tested using Kruskal-Wallis test. A p-value less than 0.05 was considered statistically significant.

2.4.1. Repeated protocol

Sites were encouraged to repeat the acquisition protocol on a different day to investigate consistency and reproducibility of frequency drift characteristics. Pearson's correlation coefficients and intraclass correlation coefficients (ICC) were calculated for the mean absolute frequency offsets between the two runs. ICC calculation was based on a two-way mixed model using absolute agreement. The median values and interquartile ranges of the mean absolute frequency offsets across all datasets and within vendors are shown in violin plots with p-values from the paired t-tests. Datasets from the first and second day were plotted against each other to allow visualized observation for consistency between the two runs. All statistical analysis was performed using R (RStudio: Integrated Development for R. RStudio, PBC, Boston, MA) (R Core Team 2020).

2.5. Convolution of frequency drift and simulated spectra

To visualize the impact of the observed frequency drifts on a typical 5-min in vivo MRS protocol, a synthetic in vivo-like spectrum was generated using FID-A (Simpson et al., 2017) density-matrix simulations and the modeling results from a recent analysis of short-TE spectra in Osprey (Oeltzschner et al., 2020; Zollner et al., 2021), including weighted signals from 18 metabolites (TE = 35 ms; 2 kHz spectral width; 2048 complex samples; 2 Hz linewidth). The simulated spectrum was convolved with the frequency trace from the first 64 TRs of the phantom scan. The convolution involved Fourier transform and shifting the zero-frequency component to the center to replicate the simulated spectrum. Frequency shifts from the 64 pre-and post-fMRI PRESS transients were applied and re-averaged to obtain the final spectra. The simulated spectra with maximum and minimum drifts across all datasets were plotted to observe how extreme frequency drift affect signal intensities. The maximum amplitude of the 2.01 ppm NAA singlet was determined to compare the change of signal intensity of the synthetic 'drift-affected' spectra before and after fMRI. Additionally, the impact of linear drift (from 0 to 50 Hz range) was demonstrated for two scenarios. First, these synthetic drift time-courses were convolved into the same simulated short-TE spectrum, and the NAA peak height reported. Second, the offset dependence of GABA editing efficiency was simulated in FID-A using 15 ms editing pulses and TE 68 ms, and the change of relative GABA signal integral was reported as a function of linear drift.

3. Results

Of the data collected from 99 scanners, 4 were excluded from the final analysis due to unexpected artifacts or corruption of data that were unable to be processed. Thus, data from 95 scanners were ultimately analyzed. No data were excluded from the repeated scans. Table 1 summarizes the numbers of sites and datasets. Table 2 summarizes scanner details. The average estimated scanner operation time per day was 7.2 ± 2.9 hours (no differences across vendors: $\chi^2 = 0.071$; $p = 0.965$), and the average age of scanner was 5.5 ± 3.8 years (no differences across vendors: $\chi^2 = 4.458$; $p = 0.108$). Low correlations were observed between operating time ($r = 0.17/0.13$) and age of scanner ($r = 0.026/0.19$) with pre-/post-fMRI frequency drift respectively, all $p > 0.05$. The median (IQR) FWHM of the water signal was 2.43 (0.01) Hz (GE: 1.90 (0.02) Hz, Philips: 2.29 (0.03) Hz, Siemens: 2.78 (0.02) Hz) for pre-fMRI PRESS and 2.44 (0.02) Hz (GE:2.02 (0.03) Hz, Philips: 2.25 (0.03) Hz, Siemens: 2.76 (0.02) Hz) for post-fMRI. The median (IQR) integral was 0.03 (2.1E-5) (GE: 0.029 (3E-4), Philips: 0.033 (2E-4), Siemens: 0.025 (3E-4)) for pre-fMRI PRESS and 0.03 (9.5E-5) (GE: 0.025 (3E-4), Philips: 0.028 (2E-4), Siemens: 0.033 (1E-4)) for post-fMRI PRESS.

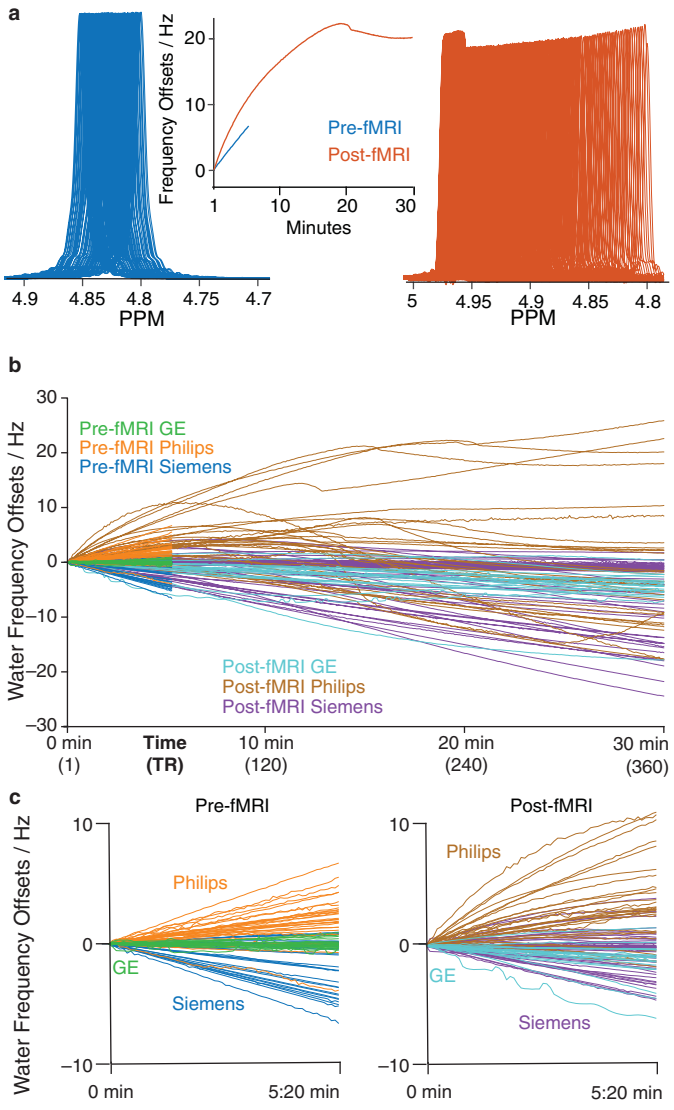

Fig. 1. a) Individual transients pre- and post-fMRI PRESS (plotted in blue and red, respectively) from one of the highest drift datasets. The frequency offset derived from modeling the water signals is plotted (middle). Three hundred sixty averages correspond to 30 min total scan duration. Panel (b) shows water offset traces for all 95 scanners before and after fMRI for GE (green and light blue), Philips (orange and brown) and Siemens (blue and purple). Panel (c) shows the pre-fMRI PRESS traces and the same period (5:20 min) for post-fMRI traces.

3.1. Frequency drift

Individual spectra from one of the highest-drifting scanners, before and after fMRI, are shown in Fig. 1a with frequency drift traces. The frequency drift traces are overlaid for all 95 initial scans in Fig. 1b. Scanners drifted by up to 7 Hz over 320 s before fMRI, and by up to 26 Hz within 30 min after 10 min of fMRI. Frequency drifts for the first 320 s before and after fMRI are shown in Fig. 1c. Violin plots of the mean absolute frequency offsets for all scanners are shown in Fig. 2a. Before fMRI, the median (IQR) was 0.44 (1.29) Hz. Mean drift across all scanners increased to 0.83 (1.29) Hz after fMRI for the first 5:20 min, and further increased to 3.15 (4.02) Hz for the full 30-min run. Average drift rates were 0.29 Hz/min and 0.43 Hz/min before and after fMRI, respectively. Due to the non-linear drift behavior of a few scanners, the

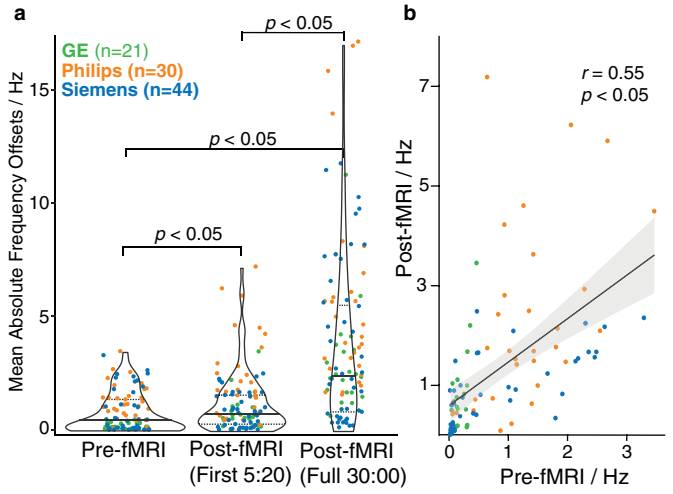

Fig. 2. a) Violin plots of mean absolute frequency offsets for all 95 scanners (median (solid line) and IQR (dashed line)); data from GE (green), Philips (orange) and Siemens (blue) are plotted. P-values show the mean values are significantly different before and after running the fMRI sequence. Panel (b) shows a scatterplot between pre-fMRI and early post-fMRI (first 5:20 min) with the confidence interval shaded in grey, in which a moderate correlation was observed.

drift rate was not determined across the full 30-min run. t-tests indicated that drift was significantly increased (t = -4.09, $p < 0.05$) after fMRI across all scanners. Correlation analysis indicated moderate correlation between drift across the first 64 transients before and after fMRI ($r = 0.55$, $p < 0.05$), as shown in Fig. 2b.

3.2. Second acquisition from repeated protocol

Sixty scanners repeated the protocol on a different day. Frequency offsets recorded on two separate days before fMRI are correlated in Fig. 3a. The same plot is shown for post-fMRI data in Fig. 3b. Within these sixty scanners, the median (IQR) frequency drift before fMRI was 0.31 (1.09) Hz and 0.33 (1.14) Hz, for the first and repeated datasets, respectively. The mean absolute frequency offsets for each session were compared pairwise within-site for repeatability and correlation. ICC and Pearson's coefficients were 0.85 and 0.75, respectively, indicating good agreement and correlation between sessions for pre-fMRI datasets. Post-fMRI, median frequency drifts on the two days were 2.55 (3.06) Hz and 2.88 (2.98) Hz, with ICC and Pearson's coefficients being 0.95 and 0.90, respectively.

3.3. Intensity changes in simulated spectra between minimum and maximum drifts

Simulated spectra convolved with 64-transient water frequency drift traces (the highest and lowest drift case for each vendor before and after fMRI) are shown in Fig. 4. The intensity of the 2.01 ppm NAA singlet in the maximum-drift cases is reduced by 5%, 28% and 28% for GE, Philips and Siemens before fMRI, respectively, and by 26%, 44% and 18% after fMRI, respectively. The impact of linear drift (of up to 50 Hz range) on the NAA peak height is shown in Fig. 5a. Since drift does not impact noise levels, these peak signal losses represent predicted losses of SNR. The effective change in GABA editing efficiency seen with linear drift is shown in Fig. 5b. Note that this Fig. reports integral, which is unaffected by lineshape convolution, to isolate this aspect of drift.

3.4. Frequency drift in an approximately three-hour long acquisition

The frequency offsets for a single 171-min post-fMRI PRESS experiment (2048 transients) are shown in Fig. 6. Gradients and bore temperatures returned to their initial state within ~10 min. The mean absolute

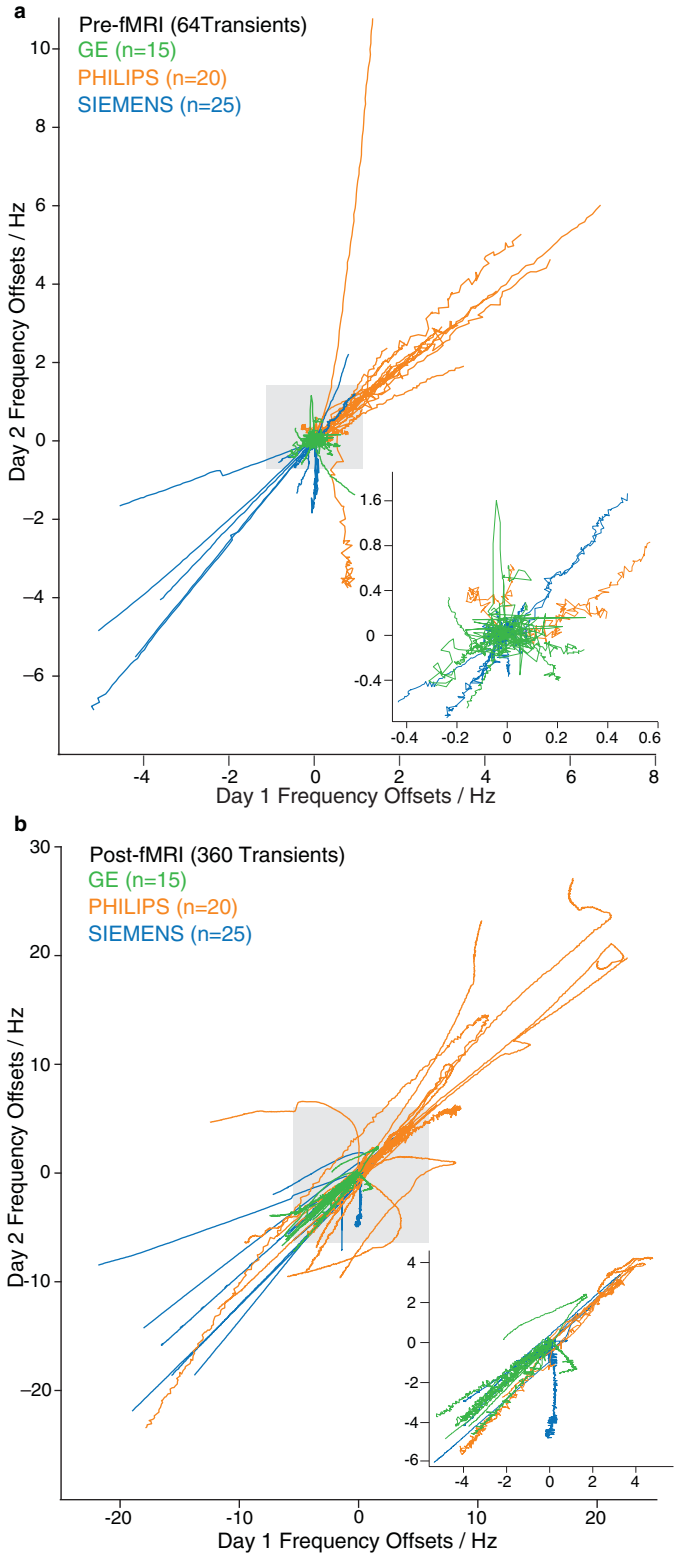

Fig. 3. Frequency offsets from day 1 against day 2 a) before fMRI and b) after fMRI, for GE (green), Philips (orange) and Siemens (blue). Inserts show only those traces that remain within the gray box on the primary plot to allow for visualization of the lower-drift traces.

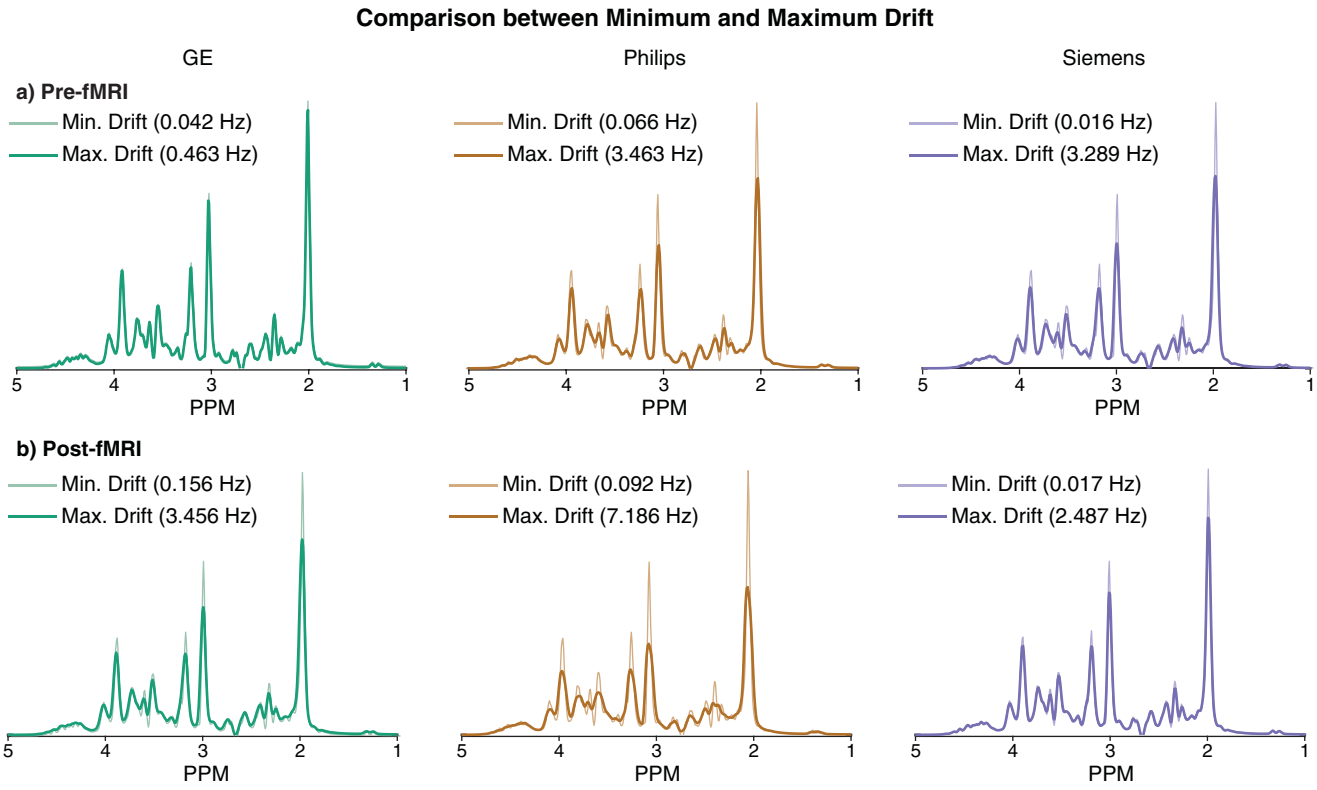

Fig. 4. Comparison of simulated spectra with frequency offsets applied between minimum and maximum drift for pre- and post-fMRI PRESS data. The minimum-drift case for each vendor (50% opacity) is overlaid with the maximum-drift case (opaque).

frequency offset was 13.9 (± 6.45) Hz and reached up to 21.5 Hz. The overall drift rate was 0.12 Hz/min but dropped to 0.03 Hz/min for the last 16 min (the last 196/2048 transients), suggesting the frequency drift approached equilibrium almost three hours after the EPI sequence. The site (G03a) provided this long acquisition data had amongst the lowest mean absolute drift in pre- and post-fMRI cases for the regular protocol, and a below average drift rate as shown in table 2.

4. Discussion

This is a large multi-site study to date that has characterized the levels of B_0 field drift in 3T MRI scanners. Results suggest that operating time and age of scanner have no significant correlations with frequency drift. Lineshapes of the acquired water signals are consistent in terms of their FWHM and integral.

4.1. Average frequency drift does not severely impact spectral data

The levels of B_0 field instability that are tolerable vary between experiments, but for the majority of MRI and MRS methods, mean offsets below 1 Hz do not have any significant impact. Including the median-drift case observed in this study, spectra are virtually indistinguishable from minimum-drift spectra because this level of instability is small compared to the typical in vivo linewidth. Moreover, the line-broadening effect seen on less stable scanners can readily be addressed using retrospective frequency correction recommended in recent consensus on MRS data processing (Near et al., 2020; Wilson et al., 2019). This is necessary even for extremely stable scanners, since it also addresses frequency and phase instability arising from subject motion.

Although the drift is significantly greater after fMRI, it typically remains in the same order of magnitude. The previous observation of field drift associated with a single run of fMRI (Harris et al., 2014), over 1 Hz/min, is above average, although falling within the range of results seen here. For a majority of scanners, although a single fMRI run does result in a less stable scanner, the extent of that impact is moderate, and the benefits of performing fMRI early in multimodal imaging protocols (particularly task-related fMRI to identify functional regions for MRS assessment) probably outweigh the detriment to MRS. However, it is important to consider that the heating effects of imaging sequences are additive, and although a single 10-min fMRI scan has limited effects, MRS performed after several runs of such scans or other EPI-based sequence such as DWI (Lange JMRI 2011) might be more seriously impacted. Furthermore, the variation among sites suggests testing drift on a specific scanner is worthwhile prior to establishing a protocol.

4.1.1. Cooling and frequency drift

While gradient cooling systems return gradient temperatures to equilibrium relatively rapidly, they do not fully prevent the dissipation of energy to elsewhere within the scanner. Cooling of other scanner parts, manifested as field drift, may require a much longer time to be stabilized. Therefore, in addition to considering the implications for sequence ordering within a protocol, one must also consider what the scanner was doing in the previous imaging session(s). For this reason, it has been suggested that running MRS scans 'from cold' will result in the greatest scanner stability especially before running B_0 field sensitive sequences. Any system feature that alters the gradient temperature during downtime (e.g., overnight to reduce energy consumption) may make pre-fMRI scans less stable than at typical daytime equilibrium; an equilibration period immediately after startup is recommended for such scanners.

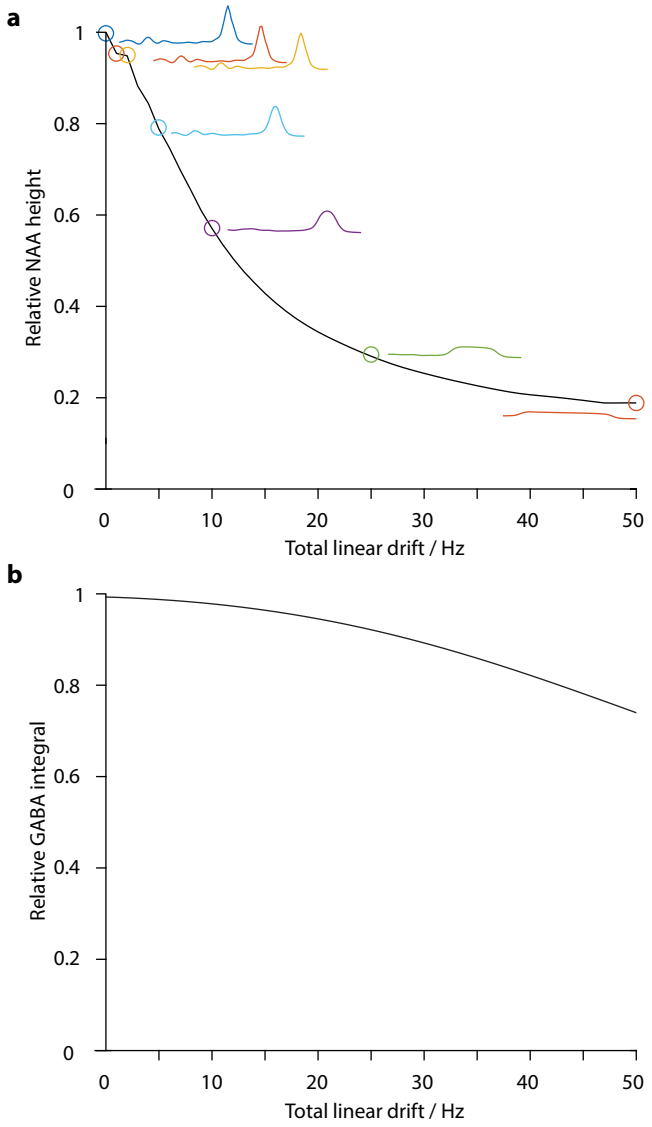

Fig. 5. Impact of linear drift. Panel (a) shows the change in simulated NAA signal height as a function of the range of linear drift. Panel (b) shows the simulated GABA integral changes as a function of the same linear drift, due to editing efficiency losses.

4.2. Frequency drift is largely consistent and reproducible within individual scanners

Over the duration of typical experiments (~10 min), the drift observed is relatively linear. Some scanners do show smooth changes of drift rate, e.g., appearing to reach a heating/cooling equilibrium and returning towards the initial center frequency. Philips scanners also illustrate some behavior that is not smooth, presumably reflecting automatic changes in an external cooling system. This dip appears between 10 and 20 min after fMRI in about two-thirds of Philips scanners. Although the extent of the dips varies, it does not seem to be related to the model or the age of the scanners. Types of cooling systems may be of interest for further study. The patterns of drift seen are also relatively reproducible (ICC » 0.9), and even smooth non-linearities in behavior are mostly reproduced in repeat measurements. This suggests that maintaining consistent scan order within protocols will reduce the variance in drift observed. This is common practice in studies, but particularly where acquiring the full protocol is in doubt, e.g., in studies of low-compliance groups, randomization of scan order is sometimes implemented. Change of SNR has been demonstrated using simulated in vivo spectra convolved with frequency traces. Results suggest that the relative change of NAA and GABA signals are minimal within 1 Hz as of lower than the median drift in a typical 5-min MRS.

4.3. Limitations

One disadvantage of the data visualizations in Figs. 1-3 is that they over-emphasize the outlier sites with large drift and tend to conceal the sites displaying very little drift. Frequency drift induced by gradient heating is a known issue, however, readings from sensors for gradient temperature monitoring have not been widely reported, while the number and locations of them also vary across vendors. Temperature readings are archived in log files, which can be retrieved retrospectively after the scan. However, the files consist of a lot of other information for the scan that make temperature retrieval more complicated. Furthermore, gradient temperatures are stored in time series and users would have to match the time of the scan with the data in log files. Real-time gradient temperature monitoring would be helpful, but it is not an available option for all scanners. Passive shim elements play a key role in heat dissipation. However, the number and bulk weight of passive shim installed are poorly reported as many of the sites that participated in this study found the information inaccessible. Finally, other studies have reported phantom temperature could be increased by approximately 1–1.5°C during a 30-min turbo spin-echo sequence (Graedel et al., 2015) and approximately 1°C during a one-hour long steady-state free precession sequence (El-Sharkawy et al., 2006). Although phantom temperature variation might have slight influence on water frequency that would, to first order, be common across all vendors, phantom heating induced by absorption of the RF energy is neglected. Human body temperature should be largely consistent throughout the scan and the effects of heating from RF is minimal.

4.4. Conclusion

While previous studies have established that scanner drift occurs, and that it can have a negative impact on the quality of data acquired (Evans et al., 2013; Harris et al., 2014; Rowland et al., 2017; Tsai et al., 2016),these studies have been carried out on a single scanner. It has not been clear to what extent these issues are generalizable to all MR scanners, or whether such issues have become over-emphasized. Overall, the results of this study are encouraging. Median levels of drift are low for cold scanners, and moderate to severe drift only appears after EPI in a small number of scanners. The implications of instability in the main magnetic field are very different for different imaging and spectroscopy sequences. It is helpful to consider the quantitative results of this study in the context of these effects. Real-time field-frequency lock for MRS acquisition is suggested to avoid drift related data instability especially after multiple long EPI acquisitions including fMRI and DTI when field drift is much more pronounced and for multi-center collaborations in which data are obtained from different scanners. In conclusion, this study measured field drift before and after 10 min of fMRI/EPI on 95 3T scanners using the MRS water signal.

Declaration of Competing Interest

Jack J. Miller would like to acknowledge the support of a Novo Nordisk Research Fellowship run in conjunction with the University of Oxford. Francisco Reyes-Madrigal has served as a speaker for Janssen (Johnson & Johnson) and AstraZeneca. Marc Thioux and Pim van Dijk were supported by The Netherlands Organization for Health Research and Development (ZonMW) and the Dorhout Mees Foundation. All other authors have no conflict of interest to declare.

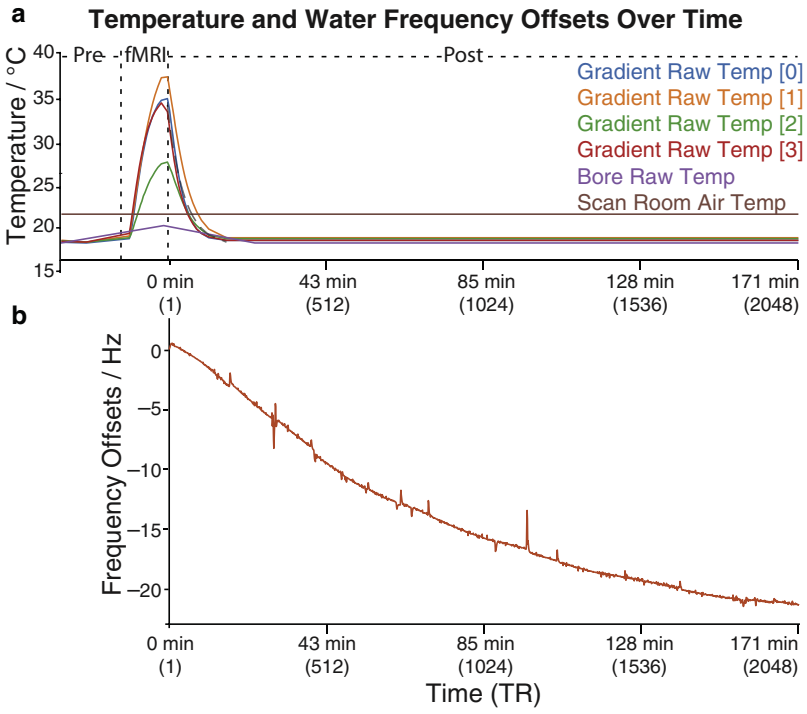

Fig. 6. Temperature change and water frequency offset before and after fMRI for the long PRESS acquisition. Panel (a) shows the corresponding gradient temperatures from sensors at different locations as well as the bore and scan room temperature. Panel (b) shows the change of frequency offsets after fMRI.

Credit authorship contribution statement

Steve C.N. Hui: Conceptualization, Methodology, Formal analysis, Writing – original draft, Writing – review & editing, Visualization, Project administration. **Mark Mikkelsen:** Methodology, Software, Writing – review & editing. **Helge J. Zöllner:** Methodology, Software, Writing – review & editing. **Vishwadeep Ahluwalia:** Validation, Resources, Writing – review & editing. **Sarael Alcauter:** Validation, Resources, Writing – review & editing. **Laima Baltusis:** Validation, Resources, Writing – review & editing. **Deborah A. Barany:** Validation, Resources, Writing – review & editing. **Laura R. Barlow:** Validation, Resources, Writing – review & editing. **Robert Becker:** Validation, Resources, Writing – review & editing. **Jeffrey I. Berman:** Validation, Resources, Writing – review & editing. **Adam Berrington:** Validation, Resources, Writing – review & editing. **Pallab K. Bhattacharyya:** Validation, Resources, Writing – review & editing. **Jakob Udby Blicher:** Validation, Resources, Writing – review & editing. **Wolfgang Bogner:** Validation, Resources, Writing – review & editing. **Mark S. Brown:** Validation, Resources, Writing – review & editing. **Vince D. Calhoun:** Validation, Resources, Writing – review & editing. **Ryan Castillo:** Validation, Resources, Writing – review & editing. **Kim M. Cecil:** Validation, Resources, Writing – review & editing. **Yeo Bi Choi:** Validation, Resources, Writing – review & editing. **Winnie C.W. Chu:** Validation, Resources, Writing – review & editing. **William T. Clarke:** Validation, Resources, Writing – review & editing. **Alexander R. Craven:** Validation, Resources, Writing – review & editing. **Koen Cuypers:** Validation, Resources, Writing – review & editing. **Michael Dacko:** Validation, Resources, Writing – review & editing. **Camilo de la Fuente-Sandoval:** Validation, Resources, Writing – review & editing. **Patricia Desmond:** Validation, Resources, Writing – review & editing. **Aleksandra Domagalik:** Validation, Resources, Writing – review & editing. **Julien Dumont:** Validation, Resources, Writing – review & editing. **Niall W. Duncan:** Validation, Resources, Writing – review & editing. **Ulrike Dydak:** Validation, Resources, Writing – review & editing. **Katherine Dyke:** Validation, Resources, Writing – review & editing. **David A. Edmondson:** Validation, Resources, Writing – review & editing. **Gabriele Ende:** Validation, Resources, Writing – review & editing. **Lars Ersland:** Validation, Resources, Writing – review & editing. **C. John Evans:** Validation, Resources, Writing – review & editing. **Alan S.R. Fermin:** Validation, Resources, Writing – review & editing. **Antonio Ferretti:** Validation, Resources, Writing – review & editing. **Ariane Fillmer:** Validation, Resources, Writing – review & editing. **Tao Gong:** Validation, Resources, Writing – review & editing. **Ian Greenhouse:** Validation, Resources, Writing – review & editing. **James T. Grist:** Validation, Resources, Writing – review & editing. **Meng Gu:** Validation, Resources, Writing – review & editing. **Ashley D. Harris:** Validation, Resources, Writing – review & editing. **Katarzyna Hat:** Validation, Resources, Writing – review & editing. **Stefanie Heba:** Validation, Resources, Writing – review & editing. **Eva Heckova:** Validation, Resources, Writing – review & editing. **John P. Hegarty II:** Validation, Resources, Writing – review & editing. **Kirstin-Friederike Heise:** Validation, Resources, Writing – review & editing. **Shiori Honda:** Validation, Resources, Writing – review & editing. **Aaron Jacobson:** Validation, Resources, Writing – review & editing. **Jacobus F.A. Jansen:** Validation, Resources, Writing – review & editing. **Christopher W. Jenkins:** Validation, Resources, Writing – review & editing. **Stephen J. Johnston:** Validation, Resources, Writing – review & editing. **Christoph Juchem:** Validation, Resources, Writing – review & editing. **Alayar Kangarlu:** Validation, Resources, Writing – review & editing. **Adam B. Kerr:** Validation, Resources, Writing – review & editing. **Karl Landheer:** Validation, Resources, Writing – review & editing. **Thomas Lange:** Validation, Resources, Writing – review & editing. **Phil Lee:** Validation, Resources, Writing – review & editing. **Swati Rane Levendovszky:** Validation, Resources, Writing – review & editing. **Catherine Limperopoulos:** Validation, Resources, Writing – review & editing. **Feng Liu:** Validation, Resources, Writing – review & editing. **William Lloyd:** Validation, Resources, Writing – review & editing. **David J. Lythgoe:** Validation, Resources, Writing – review & editing. **Maro G. Machizawa:** Validation, Resources, Writing – review & editing. **Andrei V. Manzhurtsev:** Validation, Resources, Writing – review & editing. **María L. Martinez-Gudino:** Validation, Resources, Writing – review & editing. **Jack J. Miller:** Validation, Resources, Writing – review & editing. **Heline Mirzakhanian:** Validation, Resources, Writing – review & editing. **Marta Moreno-Ortega:** Validation, Resources, Writing – review & editing. **Paul G. Mullins:** Vali-

dation, Resources, Writing – review & editing. **Shinichiro Nakajima:** Validation, Resources, Writing – review & editing. **Jamie Near:** Validation, Resources, Writing – review & editing. **Ralph Noeske:** Validation, Resources, Writing – review & editing. **Wibeke Nordhøy:** Validation, Resources, Writing – review & editing. **Georg Oeltzschner:** Validation, Resources, Writing – review & editing. **Raul Osorio-Duran:** Validation, Resources, Writing – review & editing. **Maria C.G. Otaduy:** Validation, Resources, Writing – review & editing. **Erick H. Pasaye:** Validation, Resources, Writing – review & editing. **Ronald Peeters:** Validation, Resources, Writing – review & editing. **Scott J. Peltier:** Validation, Resources, Writing – review & editing. **Ulrich Pilatus:** Validation, Resources, Writing – review & editing. **Nenad Polomac:** Validation, Resources, Writing – review & editing. **Eric C. Porges:** Validation, Resources, Writing – review & editing. **Subechhya Pradhan:** Validation, Resources, Writing – review & editing. **James Joseph Prisciandaro:** Validation, Resources, Writing – review & editing. **Nicolaas A Puts:** Validation, Resources, Writing – review & editing. **Caroline D. Rae:** Validation, Resources, Writing – review & editing. **Francisco Reyes-Madrigal:** Validation, Resources, Writing – review & editing. **Timothy P.L. Roberts:** Validation, Resources, Writing – review & editing. **Caroline E. Robertson:** Validation, Resources, Writing – review & editing. **Jens T. Rosenberg:** Validation, Resources, Writing – review & editing. **Diana-Georgiana Rotaru:** Validation, Resources, Writing – review & editing. **Ruth L O'Gorman Tuura:** Validation, Resources, Writing – review & editing. **Muhammad G. Saleh:** Validation, Resources, Writing – review & editing. **Kristian Sandberg:** Validation, Resources, Writing – review & editing. **Ryan Sangill:** Validation, Resources, Writing – review & editing. **Keith Schembri:** Validation, Resources, Writing – review & editing. **Anouk Schrantee:** Validation, Resources, Writing – review & editing. **Natalia A. Semenova:** Validation, Resources, Writing – review & editing. **Debra Singel:** Validation, Resources, Writing – review & editing. **Rouslan Sitnikov:** Validation, Resources, Writing – review & editing. **Jolinda Smith:** Validation, Resources, Writing – review & editing. **Yulu Song:** Validation, Resources, Writing – review & editing. **Craig Stark:** Validation, Resources, Writing – review & editing. **Diederick Stoffers:** Validation, Resources, Writing – review & editing. **Stephan P. Swinnen:** Validation, Resources, Writing – review & editing. **Rongwen Tain:** Validation, Resources, Writing – review & editing. **Costin Tanase:** Validation, Resources, Writing – review & editing. **Sofie Tapper:** Validation, Resources, Writing – review & editing. **Martin Tegenthoff:** Validation, Resources, Writing – review & editing. **Thomas Thiel:** Validation, Resources, Writing – review & editing. **Marc Thioux:** Validation, Resources, Writing – review & editing. **Peter Truong:** Validation, Resources, Writing – review & editing. **Pim van Dijk:** Validation, Resources, Writing – review & editing. **Nolan Vella:** Validation, Resources, Writing – review & editing. **Rishma Vidyasagar:** Validation, Resources, Writing – review & editing. **Andrej Vovk:** Validation, Resources, Writing – review & editing. **Guangbin Wang:** Validation, Resources, Writing – review & editing. **Lars T. Westlye:** Validation, Resources, Writing – review & editing. **Timothy K. Wilbur:** Validation, Resources, Writing – review & editing. **William R. Willoughby:** Validation, Resources, Writing – review & editing. **Martin Wilson:** Validation, Resources, Writing – review & editing. **Hans-Jörg Wittsack:** Validation, Resources, Writing – review & editing. **Adam J. Woods:** Validation, Resources, Writing – review & editing. **Yen-Chien Wu:** Validation, Resources, Writing – review & editing. **Junqian Xu:** Validation, Resources, Writing – review & editing. **Maria Yanez Lopez:** Validation, Resources, Writing – review & editing. **David K.W. Yeung:** Validation, Resources, Writing – review & editing. **Qun Zhao:** Validation, Resources, Writing – review & editing. **Xiaopeng Zhou:** Validation, Resources, Writing – review & editing. **Gasper Zupan:** Validation, Resources, Writing – review & editing. **Richard A.E. Edden:** Conceptualization, Methodology, Validation, Writing – review & editing, Supervision, Funding acquisition.

Acknowledgements

This work was supported by NIH grants R01 EB016089, R01 EB023963, R21 AG060245, S10 OD021726, K01 AA025306, K99 AG062230, K99 DA051315, K99 EB028828, R01 MH110270, R01-DC008871, S10 OD012336, S10 OD021648, P41 EB031771, Taiwan MOST grant 108-2410-H-038-008-MY2, JST COI grant JPMJCE1311, ERC grant #249516, DLR 01ZX1909A SySMedSUDs, Natural Sciences and Engineering Research Council of Canada RGPIN/03875-2017, CONACYT grant CF-2019-6390, The European Research Council under the European Union's Horizon 2020 Research and Innovation program (ERC StG 802998), Ariane Fillmer has received funding from the 18HLT09 NeuroMET2 project within the EMPIR programme co-financed by the Participating States and from the European Union's Horizon 2020 research and innovation programme. The contribution of Kristian Sandberg and Katarzyna Hat to this article is based upon work from COST Action CA18106, supported by COST (European Cooperation in Science and Technology). Marc Thioux and Pim van Dijk received funding from ZonMW, Dorhout Mees Foundation, Heinsius Houbolt Foundation and the European Union's Horizon 2020 research and innovation programme under the Marie Skłodowska-Curie grant agreement No 764604. NeuRA Imaging, part of the Australian National Imaging Facility, is supported by the National Collaborative Research Infrastructure Scheme. We would also like to thank Dr. Yoshihiro Noda from Keio University for his assistant on data collection.

Data and code availability statements

All data were collected prospectively using MRI phantom. They will be available on the NITRC portal in the "Big Drift" project repository (https://www.nitrc.org/projects/bigdrift/). See appendix in manuscript for more details. Data analysis was performed using MATLAB (R2020b, MathWorks, Natick, USA), and statistical analysis using R (RStudio: Integrated Development for R. RStudio, PBC, Boston, MA). All functions and packages are freely available on MATHWORKS and GITHUB.

Appendix

A subset of the data presented in this work has been made available on the NITRC portal in the "Big Drift" project repository (https://www.nitrc.org/projects/bigdrift/) for benchmark and further analyses. It is distributed freely under the Creative Commons Attribution-NonCommercial-ShareAlike license. Community members are encouraged to make use of this resource for developing and optimizing frequency drift related methods.

References

R Core Team, 2020. R: A Language and Environment for Statistical Computing. R Foundation for Statistical Computing, Vienna, Austria.

Ebel, A., Maudsley, A.A., 2005. Detection and correction of frequency instabilities for volumetric 1H echo-planar spectroscopic imaging. Magn. Reson. Med. 53, 465–469.

Edden, R.A., Barker, P.B., 2007. Spatial effects in the detection of gamma-aminobutyric acid: improved sensitivity at high fields using inner volume saturation. Magn. Reson. Med. 58, 1276–1282.

Edden, R.A., Oeltzschner, G., Harris, A.D., Puts, N.A., Chan, K.L., Boer, V.O., Schar, M., Barker, P.B., 2016. Prospective frequency correction for macromolecule-suppressed GABA editing at 3T. J. Magn. Reson. Imaging 44, 1474–1482.

Edden, R.A., Puts, N.A., Barker, P.B., 2012. Macromolecule-suppressed GABA-edited magnetic resonance spectroscopy at 3T. Magn. Reson. Med. 68, 657–661.

El-Sharkawy, A.M., Schar, M., Bottomley, P.A., Atalar, E., 2006. Monitoring and correcting spatio-temporal variations of the MR scanner's static magnetic field. MAGMA 19, 223–236.

Ernst, T., Li, J., 2011. A novel phase and frequency navigator for proton magnetic resonance spectroscopy using water-suppression cycling. Magn. Reson. Med. 65, 13–17.

Evans, C.J., Puts, N.A., Robson, S.E., Boy, F., McGonigle, D.J., Sumner, P., Singh, K.D., Edden, R.A., 2013. Subtraction artifacts and frequency (mis-)alignment in J-difference GABA editing. J. Magn. Reson. Imaging 38, 970–975.

Foerster, B.U., Tomasi, D., Caparelli, E.C., 2005. Magnetic field shift due to mechanical vibration in functional magnetic resonance imaging. Magn. Reson. Med. 54, 1261–1267.
Graedel, N.N., Polimeni, J.R., Guerin, B., Gagoski, B., Bonmassar, G., Wald, L.L., 2015. An anatomically realistic temperature phantom for radiofrequency heating measurements. Magn. Reson. Med. 73, 442–450.
Harris, A.D., Glaubitz, B., Near, J., John Evans, C., Puts, N.A., Schmidt-Wilcke, T., Tegenthoff, M., Barker, P.B., Edden, R.A., 2014. Impact of frequency drift on gamma-aminobutyric acid-edited MR spectroscopy. Magn. Reson. Med. 72, 941–948.
Helms, G., Piringer, A., 2001. Restoration of motion-related signal loss and line-shape deterioration of proton MR spectra using the residual water as intrinsic reference. Magn. Reson. Med. 46, 395–400.
Henry, P.G., van de Moortele, P.F., Giacomini, E., Nauerth, A., Bloch, G., 1999. Field-frequency locked in vivo proton MRS on a whole-body spectrometer. Magn. Reson. Med. 42, 636–642.
Keating, B., Ernst, T., 2012. Real-time dynamic frequency and shim correction for single-voxel magnetic resonance spectroscopy. Magn. Reson. Med. 68, 1339–1345.
Klose, U., 1990. In vivo proton spectroscopy in presence of eddy currents. Magn. Reson. Med. 14, 26–30.
Lange, T., Zaitsev, M., Buechert, M., 2011. Correction of frequency drifts induced by gradient heating in 1H spectra using interleaved reference spectroscopy. J. Magn. Reson. Imaging 33, 748–754.
Lee, C.Y., Choi, I.Y., Lee, P., 2018. Prospective frequency correction using outer volume suppression-localized navigator for MR spectroscopy and spectroscopic imaging. Magn. Reson. Med. 80, 2366–2373.
Marshall, I., Higinbotham, J., Bruce, S., Freise, A., 1997. Use of Voigt lineshape for quantification of in vivo 1H spectra. Magn. Reson. Med. 37, 651–657.
Mikkelsen, M., Barker, P.B., Bhattacharyya, P.K., Brix, M.K., Buur, P.F., Cecil, K.M., Chan, K.L., Chen, D.Y., Craven, A.R., Cuypers, K., Dacko, M., Duncan, N.W., Dydak, U., Edmondson, D.A., Ende, G., Ersland, L., Gao, F., Greenhouse, I., Harris, A.D., He, N., Heba, S., Hoggard, N., Hsu, T.W., Jansen, J.F.A., Kangarlu, A., Lange, T., Lebel, R.M., Li, Y., Lin, C.E., Liou, J.K., Lirng, J.F., Liu, F., Ma, R., Maes, C., Moreno-Ortega, M., Murray, S.O., Noah, S., Noeske, R., Noseworthy, M.D., Oeltzschner, G., Prisciandaro, J.J., Puts, N.A.J., Roberts, T.P.L., Sack, M., Sailasuta, N., Saleh, M.G., Schallmo, M.P., Simard, N., Swinnen, S.P., Tegenthoff, M., Truong, P., Wang, G., Wilkinson, I.D., Wittsack, H.J., Xu, H., Yan, F., Zhang, C., Zipunnikov, V., Zollner, H.J., Edden, R.A.E., 2017. Big GABA: Edited MR spectroscopy at 24 research sites. Neuroimage 159, 32–45.
Mikkelsen, M., Rimbault, D.L., Barker, P.B., Bhattacharyya, P.K., Brix, M.K., Buur, P.F., Cecil, K.M., Chan, K.L., Chen, D.Y., Craven, A.R., Cuypers, K., Dacko, M., Duncan, N.W., Dydak, U., Edmondson, D.A., Ende, G., Ersland, L., Forbes, M.A., Gao, F., Greenhouse, I., Harris, A.D., He, N., Heba, S., Hoggard, N., Hsu, T.W., Jansen, J.F.A., Kangarlu, A., Lange, T., Lebel, R.M., Li, Y., Lin, C.E., Liou, J.K., Lirng, J.F., Liu, F., Long, J.R., Ma, R., Maes, C., Moreno-Ortega, M., Murray, S.O., Noah, S., Noeske, R., Noseworthy, M.D., Oeltzschner, G., Porges, E.C., Prisciandaro, J.J., Puts, N.A.J., Roberts, T.P.L., Sack, M., Sailasuta, N., Saleh, M.G., Schallmo, M.P., Simard, N., Stoffers, D., Swinnen, S.P., Tegenthoff, M., Truong, P., Wang, G., Wilkinson, I.D., Wittsack, H.J., Woods, A.J., Xu, H., Yan, F., Zhang, C., Zipunnikov, V., Zollner, H.J., Edden, R.A.E., 2019. Big GABA II: Water-referenced edited MR spectroscopy at 25 research sites. Neuroimage 191, 537–548.
Mullins, P.G., McGonigle, D.J., O'Gorman, R.L., Puts, N.A., Vidyasagar, R., Evans, C.J., Edden, R.A.Cardiff Symposium on, M.R.S.o.G., 2014. Current practice in the use of MEGA-PRESS spectroscopy for the detection of GABA. Neuroimage 86, 43–52.
Near, J., Edden, R., Evans, C.J., Paquin, R., Harris, A., Jezzard, P., 2015. Frequency and phase drift correction of magnetic resonance spectroscopy data by spectral registration in the time domain. Magn. Reson. Med. 73, 44–50.
Near, J., Harris, A.D., Juchem, C., Kreis, R., Marjanska, M., Oz, G., Slotboom, J., Wilson, M., Gasparovic, C., 2020. Preprocessing, analysis and quantification in single-voxel magnetic resonance spectroscopy: experts' consensus recommendations. NMR Biomed. e4257.
Oeltzschner, G., Zollner, H.J., Hui, S.C.N., Mikkelsen, M., Saleh, M.G., Tapper, S., Edden, R.A.E., 2020. Osprey: Open-source processing, reconstruction & estimation of magnetic resonance spectroscopy data. J. Neurosci. Methods 343, 108827.
Poblador Rodriguez, E., Moser, P., Dymerska, B., Robinson, S., Schmitt, B., van der Kouwe, A., Gruber, S., Trattnig, S., Bogner, W., 2019. A comparison of static and dynamic B0 mapping methods for correction of CEST MRI in the presence of temporal B0 field variations. Magn. Reson. Med. 82, 633–646.
Rowland, B.C., Liao, H., Adan, F., Mariano, L., Irvine, J., Lin, A.P., 2017. Correcting for Frequency Drift in Clinical Brain MR Spectroscopy. J. Neuroimaging 27, 23–28.
Simpson, R., Devenyi, G.A., Jezzard, P., Hennessy, T.J., Near, J., 2017. Advanced processing and simulation of MRS data using the FID appliance (FID-A)-An open source, MATLAB-based toolkit. Magn. Reson. Med. 77, 23–33.
Tal, A., Gonen, O., 2013. Localization errors in MR spectroscopic imaging due to the drift of the main magnetic field and their correction. Magn. Reson. Med. 70, 895–904.
Thiel, T., Czisch, M., Elbel, G.K., Hennig, J., 2002. Phase coherent averaging in magnetic resonance spectroscopy using interleaved navigator scans: compensation of motion artifacts and magnetic field instabilities. Magn. Reson. Med. 47, 1077–1082.
Tsai, S.Y., Fang, C.H., Wu, T.Y., Lin, Y.R., 2016. Effects of Frequency Drift on the Quantification of Gamma-Aminobutyric Acid Using MEGA-PRESS. Sci. Rep. 6, 24564.
van der Veen, J.W., Marenco, S., Berman, K.F., Shen, J., 2017. Retrospective correction of frequency drift in spectral editing: The GABA editing example. NMR Biomed. 30.
Waddell, K.W., Avison, M.J., Joers, J.M., Gore, J.C., 2007. A practical guide to robust detection of GABA in human brain by J-difference spectroscopy at 3 T using a standard volume coil. Magn. Reson. Imaging 25, 1032–1038.
Weiner, M.W., Veitch, D.P., Aisen, P.S., Beckett, L.A., Cairns, N.J., Green, R.C., Harvey, D., Jack Jr., C.R., Jagust, W., Morris, J.C., Petersen, R.C., Salazar, J., Saykin, A.J., Shaw, L.M., Toga, A.W., Trojanowski, J.Q.Alzheimer's Disease Neuroimaging, I., 2017. The Alzheimer's Disease Neuroimaging Initiative 3: Continued innovation for clinical trial improvement. Alzheimers Dement 13, 561–571.
Wilson, M., 2019. Robust retrospective frequency and phase correction for single-voxel MR spectroscopy. Magn. Reson. Med. 81, 2878–2886.
Wilson, M., Andronesi, O., Barker, P.B., Bartha, R., Bizzi, A., Bolan, P.J., Brindle, K.M., Choi, I.Y., Cudalbu, C., Dydak, U., Emir, U.E., Gonzalez, R.G., Gruber, S., Gruetter, R., Gupta, R.K., Heerschap, A., Henning, A., Hetherington, H.P., Huppi, P.S., Hurd, R.E., Kantarci, K., Kauppinen, R.A., Klomp, D.W.J., Kreis, R., Kruiskamp, M.J., Leach, M.O., Lin, A.P., Luijten, P.R., Marjanska, M., Maudsley, A.A., Meyerhoff, D.J., Mountford, C.E., Mullins, P.G., Murdoch, J.B., Nelson, S.J., Noeske, R., Oz, G., Pan, J.W., Peet, A.C., Poptani, H., Posse, S., Ratai, E.M., Salibi, N., Scheenen, T.W.J., Smith, I.C.P., Soher, B.J., Tkac, I., Vigneron, D.B., Howe, F.A., 2019. Methodological consensus on clinical proton MRS of the brain: Review and recommendations. Magn. Reson. Med. 82, 527–550.
Zollner, H.J., Povazan, M., Hui, S.C.N., Tapper, S., Edden, R.A.E., Oeltzschner, G., 2021. Comparison of different linear-combination modeling algorithms for short-TE proton spectra. NMR Biomed. 34, e4482.